6286–6300 *Nucleic Acids Research, 2010, Vol. 38, No. 18* *Published online 14 May 2010*
doi:10.1093/nar/gkq385

The protein–DNA contacts in RutR·*carAB* operator complexes

Phu Nguyen Le Minh[1], Indra Bervoets[1], Dominique Maes[2] and Daniel Charlier[1,*]

[1]Erfelijkheidsleer en Microbiologie and [2]Structural Biology Brussels, Vrije Universiteit Brussel (VUB) and Vlaams Interuniversitair Instituut voor Biotechnologie (VIB), Pleinlaan 2, B-1050 Brussel, Belgium

Received January 12, 2010; Revised April 18, 2010; Accepted April 29, 2010

ABSTRACT

Pyrimidine-specific regulation of the upstream *car*P1 promoter of the carbamoylphosphate synthase operon of *Escherichia coli* requires numerous *trans*-acting factors: the allosteric transcription regulator RutR, the nucleoid-associated protein integration host factor, and the trigger enzymes aminopeptidase A and PyrH (UMP-kinase). RutR, a TetR family member, binds far upstream of *car*P1. Here, we establish a high-resolution contact map of RutR•*car*P1 complexes for backbone and base-specific contacts, analyze DNA bending, determine the DNA sequence specificity of RutR binding by saturation mutagenesis, demonstrate that uracil but not thymine is the physiologically relevant ligand that inhibits the DNA binding capacity of RutR and build a model of the RutR·operator DNA complex based on the crystal structures of RutR and of the DNA-bound family member QacR. Finally, we test the validity of this model with site-directed mutagenesis of the helix–turn–helix DNA binding motif and *in vitro* binding studies with the cognate purified mutant RutR proteins.

INTRODUCTION

RutR (b1013, *ycdC*) was originally identified as the transcriptional regulator of the *rutABCDEFG* operon (b1012), encoding a novel pathway for pyrimidine utilization discovered in *Escherichia coli* (1). Additional binding sites for RutR on the *E. coli* chromosome were identified by using genomic SELEX (systematic evolution of ligands by exponential enrichment) and ChIP-chip (chromatin immunoprecipitation in combination with DNA microarray; 2,3). Curiously, only 6 of the 20 identified binding sites for RutR are located in intergenic regions. The RutR binding site with the highest affinity is located in the control region of the *carAB* operon, encoding carbamoylphosphate synthase, far upstream of the transcription start of the *car*P1 promoter (Figure 1). Other regulatory targets of RutR are genes of pyrimidine and purine catabolism, synthesis of glutamine, and transport of glutamate. From these binding sites a 16 bp palindromic consensus RUT box sequence was derived (Figure 1b) and a sequence logo was constructed (2,3).

The structure of the RutR protein has been solved even before its function was known (pdb1PB6). RutR is a member of the widespread TetR-family of transcriptional regulators with members in both Bacteria and Archaea (4). TetR-like regulators are two-domain proteins with a signal receiving effector binding domain and a DNA-binding domain with a helix–turn–helix (HTH) motif that transduces the signal. They regulate various genes involved in diverse processes including multidrug resistance, biosynthesis of antibiotics, osmotic stress, biofilm formation, pathogenicity of Gram-negative and Gram-positive bacteria and various catabolic pathways. They are particularly abundant in microbes exposed to environmental changes. All TetR members of which the function is known are repressors and effector binding results in their release from the DNA. The best overall structural resemblance of RutR is with the transcriptional regulator AefR from *Pseudomonas syringae* that controls epiphytic fitness and the production of *N*-acyl homoserine lactone (AHL), a putative quorum sensing signal (5). However, the highest degree of sequence conservation in the HTH DNA-binding domain is with QacR, a multidrug-binding regulator from *Staphylococcus aureus* (6).

Unlike most other organisms, *E. coli* has only one carbamoylphosphate synthase that ensures the production of carbamoylphosphate (CP), a precursor common to the *de novo* synthesis of arginine and pyrimidines. Therefore, the *carAB* operon occupies a key position, at the intersection of the biosynthesis of building blocks for proteins and nucleic acids. This distinguishing feature is reflected in the complex patterns of enzymotropic and genotropic control

*To whom correspondence should be addressed. Tel: +32 2 6291342; Fax: +32 2 6291345; Email: dcharlie@vub.ac.be

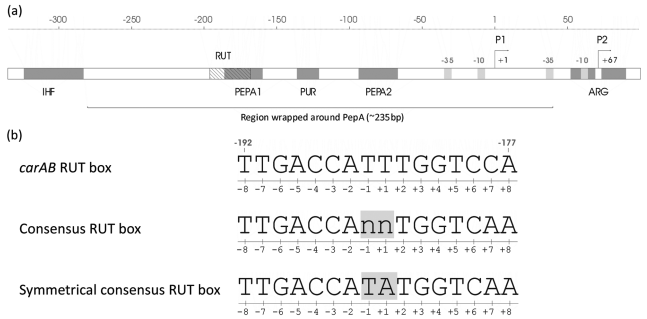

Figure 1. (**a**) Schematic view of the *carAB* control region with indication of the −10 and −35 core promoter elements and startpoint (arrow) of *car*P1 and *car*P2, and the target sites for the various DNA-binding proteins involved in arginine, purine and pyrimidine-specific regulation. PEPA1 and PEPA2 represent two zones that are strongly protected against DNaseI upon PepA binding, but the zone of contact is much larger (alteration of zones of protection and hyperreactivity for DNase I) and binding of hexameric PepA results in the wrapping of about 235 bp, as indicated by the horizontal line (18). (**b**) DNA sequence alignment of the consensus RutR binding site as determined by Shimada *et al.* (3), the 16 bp conserved RutR binding site in the *carAB* control region, and the fully symmetrical RutR consensus site used in this work.

of CP production (7, http://www.ecosal.org). The *carAB* operon is transcribed from two promoters in tandem (8,9). The downstream promoter *car*P2 is essentially repressed by hexameric arginine-bound ArgR that binds to two ARG boxes, partially overlapping the promoter, and sterically excludes the binding of RNA polymerase (10–12). Regulation of the *car*P1 promoter activity is more complex and relies on a combination of DNA-binding protein-dependent and -independent mechanisms. The latter comprise stringent control and UTP-sensitive reiterative transcription initiation (stuttering; 8,13). The *car*P1 control region harbours binding sites for the transcriptional regulators PurR (purine repressor) and RutR (pyrimidine utilization regulator), and for the architectural proteins IHF (integration host factor) and PepA (aminopeptidase A, a trigger enzyme; Figure 1a; 2,14–18). Furthermore, the trigger enzyme PyrH (UMP-kinase) appears to be involved as well and might be recruited by protein–protein contact (19–21). Numerous elements of the *car*P1 regulatory mechanism have been identified, but it is not yet known how they all fit precisely together. PepA is a crucial element in both pyrimidine and purine-specific regulation of *car*P1 activity and was recently shown to wrap about 230 bp of the *car*P1 operator DNA (Figure 1; 16,18).

This article contributes to the unravelling of the RutR–*car*P1 operator interactions. Dimeric RutR was previously shown to bind to the *carAB* control region in a uracil and thymine-sensitive manner and to protect an ~30 bp strech against DNaseI digestion (2). However, further molecular details of the RutR–operator interaction are lacking and the role of the potential effector molecules for RutR necessitates further investigations. Here, we establish a high-resolution contact map of the RutR–*car*P1 operator interaction comprising both backbone and base-specific contacts, groove and group-specific interactions and analyze RutR-induced DNA bending. We propose a model for the RutR·*car*P1 complex showing interacting pairs of amino acids and base-specific groups or phosphates. The validity of this model is tested with site-directed mutagenesis and *in vitro* DNA binding studies of six purified mutant RutR proteins bearing a single amino acid substitution in the DNA-binding motif. Finally, we demonstrate that uracil but not thymine is the physiologically relevant effector molecule that disrupts RutR·DNA complexes.

MATERIALS AND METHODS

DNA manipulations, plasmid constructions and site-directed mutagenesis

Escherchia coli MG1655 [λ^-, F^-, *rph*-1, *rfb*-50, *ilvG*$^-$, *fnr*$^-$] (Netherlands Culture Collection of Bacteria; NCCB, Utrecht, The Netherlands) was used for DNA amplification. All oligonucleotides used in this work are listed in the Supplementary Data (Supplementary Table S1). All ligation products were transformed in *E. coli* strain DH5α [F^- ϕ80*lacZ*ΔM15 *Δ*(*lacZYA-argF*)U169 *hsd*R17U (rK^- mK^+) *phoA supE*44 *recA1 endA1 gyrA*96 *thi-1 relA*1]. Plasmids pBend2 (22) and pFW-carP1 (16) are described; pET24a was from Novagen. The pBendRUT vector for the circular permutation assay was obtained by inserting the annealed pair of oligonucleotides DC647f and DC648r bearing sticky XbaI sites at the ends into the unique XbaI site of pBend2. To construct the vector pET24-rutRHis_6 for overexpression of his-tagged RutR protein, the coding part of the *E. coli rutR* gene (without the stop codon) was amplified using genomic DNA of strain MG1655 as a template and the oligonucleotides Fw-NdeI-2aa-rutR and Rv-XhoI-H-rutR as primers. The amplicon was digested with the enzymes NdeI and XhoI and ligated in similarly digested and dephosphorylated pET24a vector DNA. Single amino acid substitution mutants were constructed by site-directed mutagenesis performed according to the overlap PCR method (23). All constructs were verified by DNA sequencing.

Overexpression and purification of RutR-His_6 and single amino acid substitution mutants of RutR-His_6

C-terminally hexa-histidine tagged RutR was purified from a 300 ml culture of strain BL21(DE3) [F^- *ompT hsdS*$_B$ (r_B^- m_B^-) *gal dcm* (DE3)] (Novagen) transformed with the plasmid pET24-rutRHis_6 grown at 30°C in complex medium supplemented with kanamycin till a cell density of 6×10^8 cells ml^{-1}, induced with isopropyl-β-D-thiogalactopyranoside (IPTG) at 1 mM and grown overnight. The purification scheme was based on the previously described protocol (2). Briefly, lysate obtained from sonicated harvested cells was loaded onto a desalting column (Hitrap desalting, GE Healthcare) prior to loading onto a HisTrap column (HistrapFF, GE Healthcare) allowing Ni^{2+} ion affinity chromatography purification of the His-tagged protein. Equilibration of the column was performed with 20 mM sodium phosphate buffer, 0.5 M NaCl, 40 mM imidazole

pH 7.4. Elution of RutR-His_6 was obtained by applying a linear gradient from 40 to 500 mM imidazole. Fractions containing RutR-His_6 protein were identified by SDS–PAGE and mobility shift assays with the *carAB* operator region as probe. Fractions containing RutR-His_6 at a degree of purity >95% were pooled and were submitted to dialysis in the storage buffer, 50 mM Tris–HCl, 200 mM KCl, 10 mM $MgCl_2$,1 mM EDTA, 1 mM DTT, prior to finally being stored in the same buffer with 12.5% glycerol.

Electrophoretic mobility shift assays

Electrophoretic mobility shift assay (EMSA) experiments were performed either with single 5′-end labelled PCR amplicons or with 46-bp oligonucleotide duplexes. The latter were generated by annealing of complementary oligonucleotides (Supplementary Table S1), of which one was 5′-end labelled with [γ-^{32}P]-ATP by T4 polynucleotide kinase. Single 5′-end labeled DNA fragments were generated by PCR amplification with pFW-carP1 plasmid DNA as template and as primers various pairs of oligonucleotides, one of which was 5′-end labelled with [γ-^{32}P]-ATP and T4 polynucleotide kinase. The 162-bp fragment was generated with the primer pair AB6 and PURbend, it comprises the operator stretch from −113 to −271 upstream of the start of *car*P1 transcription. The 116-bp fragment was generated with the primer pair DC663f and DC664r, it encompasses the operator stretch from −128 to −244. Separation of RutR–DNA complexes from free DNA molecules was performed on 6% and 8% polyacrylamide gels for the DNA fragments and the 46-bp duplexes, respectively. All binding reactions were performed at 37°C, in RutR binding buffer [50 mM Tris–HCl (pH 7.8), 50 mM NaCl, 3 mM Mg acetate, 0.1 mM EDTA, 0.1 mM dithiothreitol, 25 mg ml^{-1} BSA], and in the presence of a large excess of non-specific competitor DNA (25 µg ml^{-1} sonicated herring sperm DNA). Migration was carried out for 3 h at 8 V cm^{-1} in TEB buffer (89 mM Tris, 89 mM boric acid, 0.25 mM EDTA). Apparent dissociation equilibrium constants (K_D) and inhibition constants of effector molecules were determined by densitometry of the free DNA bands as a function of the protein and ligand concentration, respectively, and are the mean value of at least two assays. Data analysis was performed as described previously (24).

Footprinting and binding interference analysis

DNase I and hydroxyl radical footprinting, phosphate ethylation, pre-methylation, depurination and depyrimidation binding interference were all performed with single 5′-^{32}P-end labelled DNA fragments as described previously (12). In-gel footprinting with the 1, 10-phenanthroline-copper ion [$(OP)_2$-Cu^+] was performed as described (25). All binding reactions were done in RutR binding buffer except for the hydroxyl radical footprinting, which was performed in Bis-Tris buffer as described (12). Reference ladders were generated by chemical sequencing methods (26).

DNA bending test

To analyze intrinsic and RutR-induced bending of the *car*P1 operator, we used the circular permutation assay (21). A set of six fragments of identical length bearing the RutR binding site at various distances from the extremities were generated by PCR amplification with pBendRUT plasmid DNA as template and the oligonucleotide pairs EP15-EP16r, EP17-EP18r, EP9-EP10r, EP19-EP20r, EP21-EP22r and DC647f-EP31r as primers. EMSAs with purified RutR-His_6 binding to these various fragments were performed on 8% acrylamide gels.

Model building

The Cα's of the HTH motif (amino acid range 17–60, RutR numbering) of one monomer of each molecule were superimposed using the LSQ-superpose option in the program Wincoot (27). Figure 8 was drawn using the software UCSF Chimera (28).

RESULTS

RutR contacts three helical turns of the *car*P1 operator on one face of the DNA helix

Previously, RutR was shown to protect against DNase I an ~30-bp long stretch of the top strand (coding strand) of the *car*P1 control region, from position −268 to −296 upstream of the TTG initiation codon of *carA* translation (−168 to −196 upstream of the start of *car*P1 transcription; Figure 1a; 2). We have applied a battery of *in vitro* protection and pre-modification binding interference techniques that provide a detailed map of both backbone and base-specific contacts of RutR with both DNA strands. Representative autoradiographs are shown for one strand only (Figure 2). A summary of the results obtained with all techniques and for both strands is provided in Figure 3.

DNase I footprinting of RutR–*carAB* complexes (Figure 2a) revealed on both strands an ~26- to 28-nt long stretch of protection, slightly offset in the 3′-direction on opposite strands, indicating that RutR covers nearly three helical turns of the operator (from −171 to −200 upstream of the start of transcription, Figure 3). This region comprises the conserved 16 bp RutR box, and extends about 8 bp more upstream and 6 bp further downstream. However, the limits of this region are difficult to determine precisely in the very A+T rich sequences immediately flanking the RutR box due to the low cutting activity of DNase I, a sensor of minor groove geometry. Clear-cut RutR-induced hyperreactivity for DNase I was not observed. This result gives an early indication that RutR binding does not cause a profound DNA deformation by bending or kinking (see bending analysis below).

To delimit the RutR binding site more precisely, we performed in-gel footprinting of the RutR–operator complex with the 1, 10-phenanthroline-copper ion [$Cu(OP)_2$-Cu^+] (29). This resulted in the protection on both strands of a 24- to 26-nt long stretch, slightly offset in the 3′-direction on opposite strands (Figures 2b and 3), and a global zone of protection extending from −170 to −197 that

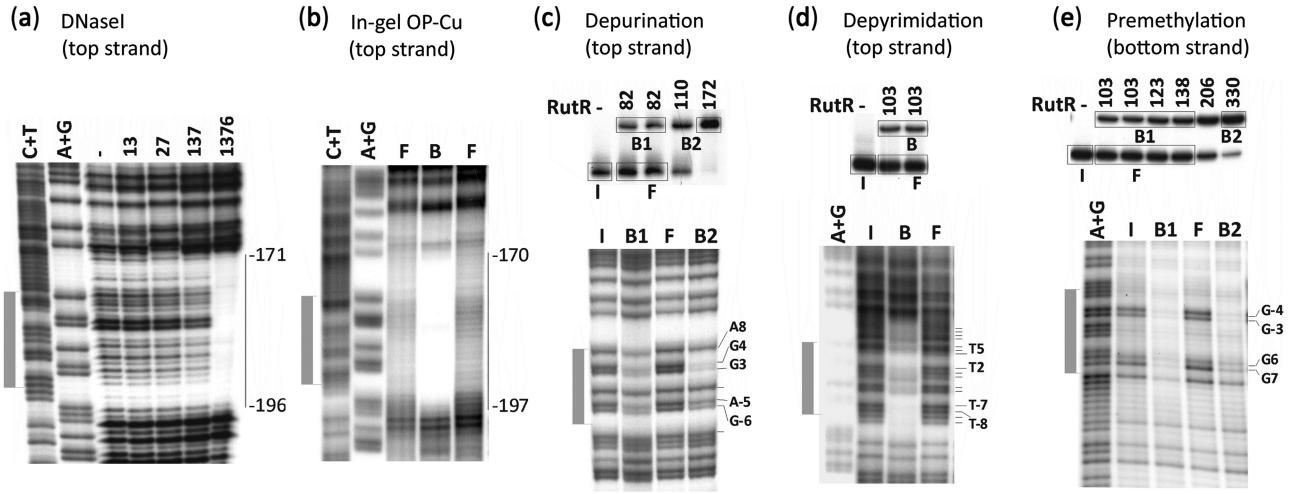

Figure 2. Representative autoradiographs of *in vitro* binding protection and premodification binding-interference studies of RutR binding to the *car*P1 control region with the top strand revealed. (**a**) DNase I footprinting. A+G and C+T represent the Maxam–Gilbert sequencing ladders. Regions that are protected against DNase I cleavage are indicated with a vertical line. The conserved 16 bp RutR binding site is indicated with filled bar. (**b**) In-gel Cu-phenanthroline footprinting, (**c**) depurination missing contact probing (**d**) depyrimidation missing contact probing, (**e**) pre-methylation binding interference. In all pre-modification binding-interference experiments, sparingly modified DNA was incubated with various amounts of RutR and RutR–DNA complexes were separated from free DNA by gel electrophoresis in native conditions. Input (I), free DNA (F) and RutR-bound DNA (B) were eluted from the gel, cleaved at the modified positions and the reaction products analyzed by gel electrophoresis in denaturing conditions. A summary of the effects for both strands is given in Figure 3.

is in good agreement with the DNase I footprint. Hydroxyl radical footprinting (30) of RutR–operator complexes revealed on each strand three patches of protection of 3 to 5 nt long, the centres of which are approximately one helical turn apart and offset by two to four nucleotides in the 3′-direction on complementary strands (Figure 3). Such a pattern is strongly suggestive of binding to one face of the DNA molecule.

To gather further information on RutR–DNA backbone contacts, we performed phosphate ethylation interference assays with operator DNA randomly modified by *N*-ethyl-nitroso urea, in such manner that statistically each molecule was ethylated at a single phosphate hydroxyl group only (31). This mixture of modified DNA molecules was subsequently separated on the basis of the affinity for RutR by an EMSA. The different populations of DNA molecules were then recovered from the gel, cleaved at the modified positions and analyzed by gel electrophoresis in denaturing conditions. The formation of a phosphate triester adds an ethyl group and removes a negative charge. A reduction in the RutR binding upon ethylation can thus be caused either by a local steric interference or by the loss of an electrostatic interaction. The information obtained with this technique is therefore complementary to the footprinting techniques described above, which show regions of the operator being shielded by the regulator from the attack (enzymatic or chemical) by an external agent. On both strands the phosphate groups that upon ethylation interfere significantly to strongly with RutR binding are clustered in three patches of three to four, and are offset by a few nucleotide towards the 3′-end on complementary strands (Figure 3). This pattern corresponds rather well to the distribution of ribose residues that are protected by RutR against the hydroxyl radical attack, and confirms that RutR contacts three helical turns of the DNA. The strongest reduction in RutR binding occurred upon ethylation of the phosphate group 5′ to the bases G+3, G+4 and T-8 of the top strand, and the symmetrically related positions G-4, G-3 and T+8 of the bottom strand. They all belong to the 16 bp highly conserved part of the RutR binding site (RutR box) and, furthermore, they are mostly located to the 5′-side of bases that are important for RutR binding (see below).

High-resolution contact mapping of base-specific RutR–*car*P1 operator interactions

The sequence comparison of the 20 binding sites for RutR on the *E. coli* chromosome has allowed Shimada *et al.* (3) to deduce a 16 bp consensus sequence for the RutR target—TTGACCANNTGGTGAA—and to establish a sequence logo in which the A•T and T•A base pairs in respective position −5 and +5 of the binding site show the highest degree of conservation (Figure 1). They are, therefore, supposed to play a crucial role in the sequence-specificity of RutR binding.

To experimentally identify the critical points of contact between RutR and base-specific groups exposed in the major and minor grooves of the *car*P1 operator, we performed pre-methylation binding interference experiments and missing contact probing assays with sparingly depurinated and depyrimidated DNA (32). These techniques are based on the creation of a pool of DNA molecules with on average one base-specific modification per molecule. The subsequent separation of low and high affinity molecules in an EMSA and their analysis by gel electrophoresis in denaturing conditions after cleavage at the methylated or abasic positions allows to distinguish

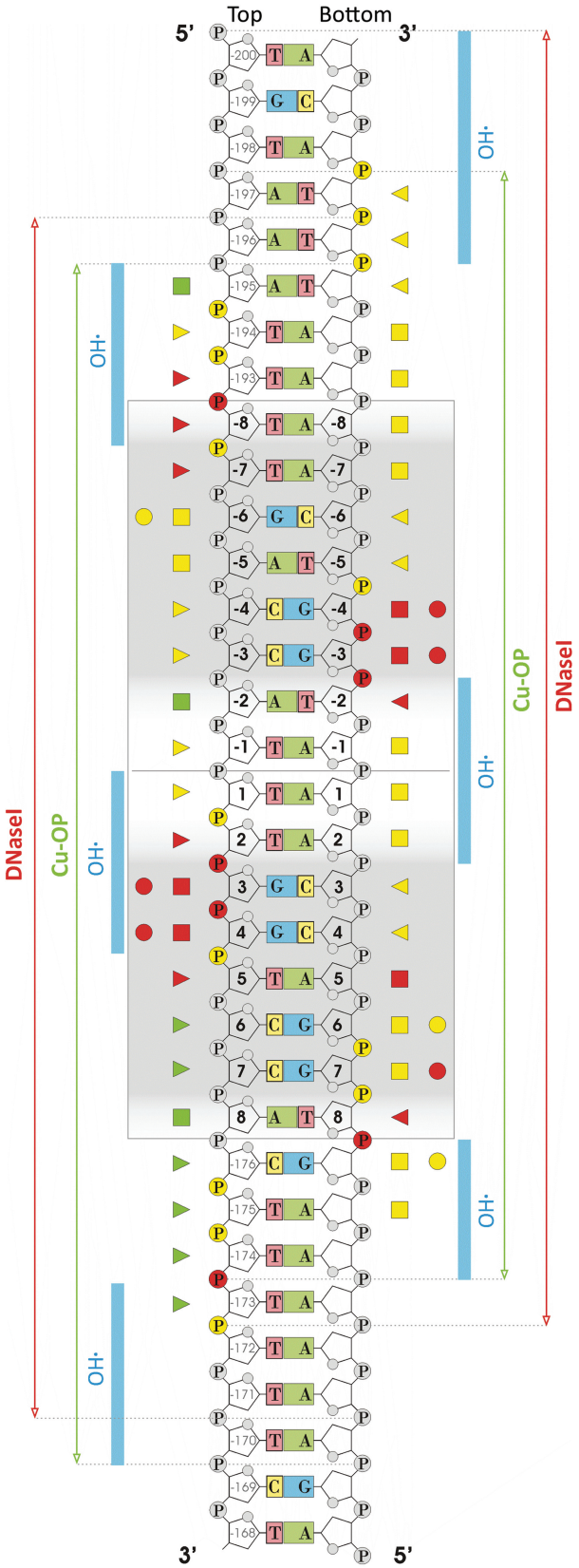

Figure 3. Nucleotide sequence of the RutR binding site in the *car*P1 control region and compilation of the results of the various footprinting and pre-modification binding-interference techniques. The regions protected against cleavage by DNase I, the 1, 10-phenanthroline-copper ion, and hydroxyl radicals are indicated with red, green, and blue lines, respectively. Phosphates that upon ethylation interfere with RutR binding are colored red for strong effects and yellow for moderate effects. Squares and triangles represent purines and pyrimidines, respectively, which upon removal negatively affect RutR binding. Balls represent purine residues that negatively affect RutR binding when methylated at the N^7 position of guanine in the major groove. Red, yellow and green symbols represent strong, moderate and weak effects, respectively. Gray-shaded areas correspond to major groove segments of the operator contacted by RutR.

positions that are important or even crucial for binding (underrepresented in the bound form) from positions that are irrelevant for binding (evenly distributed over free and bound forms).

Sparingly depurinated and depyrimidated operator DNA was prepared in acidic conditions and by hydrazine treatment, respectively (26). Interference effects observed upon base removal are generally considered to represent direct effects, reflecting a direct or water-mediated interaction between the base and the interacting protein (in contrast to what may happen with modifications such as methylation that add of a bulky group to the base). However, an indirect effect may still occur if the creation of an abasic position would significantly alter the local DNA conformability. From the depurination experiments, we may conclude that the removal of either one of eight guanines and 13 adenines significantly reduces RutR binding (Figures 2c and 3). The most salient effects were observed upon removal of G+3 and G+4 of the top strand and G-3, G-4 and A+5 of the bottom strand. Similarly, we established that the removal of either one of eight cytosines and 17 thymines significantly lowers the affinity for RutR (Figures 2d and 3). Here, the strongest effects were observed for the stretch T-9 to T-7, and the residues T+2 and T+5 of the top strand, and T-2 and T+8 of the bottom strand. Notice that the majority of these effects occur within the 16 bp RutR box, but contacts with a few flanking bases on either side also contribute to the interaction.

Dimethylsulphate (DMS) was used to methylate the N^7 position of guanine exposed in the major groove, and the N^3 position of adenine, exposed in the minor groove (26). The subsequent piperidine induced β-elimination resulted in preferential cleavage of the phosphodiester bonds at modified guanine residues. Methylation of a purine adds a methyl group and a positive charge, and removes a potential hydrogen bond acceptor. Therefore, pre-methylation binding interference can result from steric exclusion of RutR binding, or from a change in the resonance state of the purine ring such that the regulator can no longer recognize the modified base. Pre-methylation at any of seven guanine residues significantly reduced RutR binding (Figures 2e and 3). The strongest effects were observed for G+3 and G+4 of the top strand and G-4, G-3 and G+7 of the bottom strand. Significant piperidine-induced cleavage associated with an under representation in the bound form was also observed for two methylated A residues, at position −2 and +8 of the top strand, suggestive of minor groove contacts at these positions of the RutR binding site (Figure 3).

Notice that all these residues also interfered strongly to moderately with RutR binding upon removal of the purine base, in the missing contact probing assay. Therefore, it appears that RutR interacts most tightly with two successive major groove segments of the operator, aligned on the same face of the helix.

Sequence specificity of RutR binding

To further determine the sequence specificity of RutR binding, we studied complex formation with a 46-bp oligonucleotide duplex containing a fully symmetrical 16-bp RutR consensus binding site (Figure 1b) flanked by the 15-bp stretches that surround the RutR binding site in the *car*P1 control region, and a series of double bp substitutions thereof, bearing symmetrical substitutions in the two half-sites. These mutations affect four positions of the binding site (positions 1, 3, 4 and 5). From the high-resolution contact mapping it appears that positions 3, 4 and 5 are contacted through the major groove, whereas at position 1, in the center of the binding site, the minor groove is facing RutR. A saturation mutagenesis was performmed for positions 3, 4 and 5 that appear to be important for complex formation as indicated by the missing contact probing and premethylation binding interference. Furthermore, position 5 shows the highest degree of sequence conservation in the RutR-binding site DNA sequence logo (3).

An example of such a binding analysis is presented for position 4 of the RutR box (Figure 4). Average apparent K_D values and relative K_D values for all the mutants are summarized in Table 1. Most remarkably, a survey of the relative binding affinities indicates that substituting A·T for C·G at position 3 and even more so at position 4, has the largest negative effect of all three possible substitutions. This is unexpected, given that in the major groove A·T is more similar to C·G than is T·A (Figure 4). Possibly, this important negative effect on complex formation might be occasioned by the specific position of the hydrophobic methyl group of the thymine residue. To verify this hypothesis, we replaced thymine by uracil (substitution of A·U/U·A for C·G/G·C). The results indicate that substituting A·U for C·G at position 4 has a smaller negative effect on complex formation than A·T, and is similar to U·A (and T·A). Therefore, we may conclude that the C^5 methyl group of a thymine residue at position +4 of the top strand (and the symmetrically related position −4 of the bottom strand) strongly interferes with RutR binding, likely by exerting a steric hindrance on DNA conformability and/or on the establishment of one or more nearby contacts. Although this was not tested here, it is likely that the same explanation holds for position 3, even though the difference in binding to A·T and T·A is less pronounced at this position (Table 1).

No sequence preference can be detected at the center of the RutR binding site (position −1/+1) in the previously established sequence logo (3). In the minor groove, A·T and T·A are nearly indistinguishable, but different from C·G and G·C. Sequence conservation in the minor groove is generally indicative of DNA deformations and it has been observed repeatedly that the substitution of a weak by a strong base pair in the center of a binding site has a negative effect on complex formation, due to the steric hindrance exerted by the exocyclic amino group at position C^2 of the guanine ring on minor groove compression upon DNA bending. As indicated in Table 1, replacing the T·A/A·T base pairs at position −1/+1 of the RutR consensus binding site by G·C/C·G or I·C/C·I (I is similar to G but is missing the amino group at C^2) had only a minor effect on complex formation. This result is compatible with the DNase I footprinting data (lack of clear-cut hyperreactivity) and the small RutR-induced bending angle calculated from the circular permutation assay (see below).

Groove-specific ligand binding interference

EMSAs performed with the 162-bp DNA fragment comprising the operator stretch from −113 to −271 upstream of the start of *car*P1 transcription indicated that RutR binds to the *car*P1 operator, thereby forming a single complex with a distinct migration velocity and an apparent equilibrium dissociation constant of ∼10 nM (Figure 5a). This binding proved to be very resistant to increasing concentrations of non-specific competitor DNA and is therefore highly specific (data not shown). Only at the highest RutR concentrations used could a second supershifted complex be observed. This is likely due to additional non-specific binding or the formation of RutR aggregates. To further analyze the importance of minor and major groove specific contacts in the binding of RutR to the *car*P1 operator, we performed EMSAs in the presence of groove-specific ligands. Distamycin A is a basic oligopeptide with three *N*-methylpyrrole rings that interacts non-covalently with the minor groove, especially of A+T rich sequences (33). In contrast, methyl green interacts with the hydrophobic surfaces in the major groove segments. Incubation of the *car*P1 operator fragment with a fixed amount of RutR and increasing concentrations of ligand resulted in a gradual decrease in complex formation in the EMSAs (Figure 5b and c) with 50% binding inhibition at 15 μM distamycin A or 290 μM methylgreen. This result indicates a contribution of both major and minor groove determinats in the formation of RutR·*carAB* operator complexes and is reminiscent of our previous observations made with the binding of ArgR to the *carAB* control region (12).

DNA bending analysis

Every one of the previously identified DNA-binding proteins that bind to the *carAB* control region (ArgR, PurR, IHF, PepA) induces a pronounced bending (97–144°) or even wrapping (±260° wrapping around hexameric PepA) of the operator (16,18, and unpublished observations from this laboratory). To analyze potential RutR-induced bending of the RutR box, we performed a circular permutation assay (22). Six fragments of identical length, but bearing the target site at a different position, were generated by PCR amplification with pBendRUT as template and different combinations of pairs of oligonucleotides as primers (see 'Materials and Methods' section).

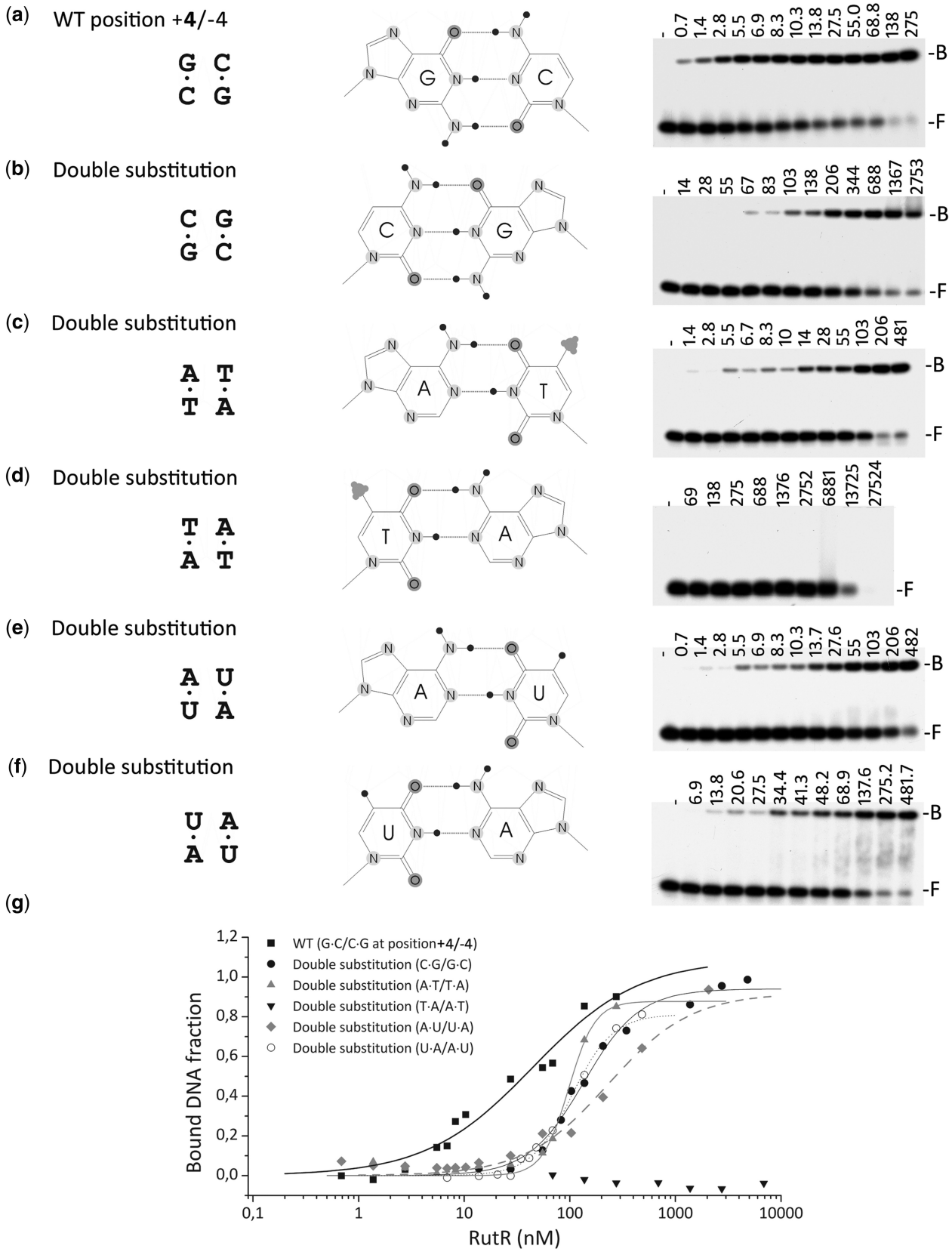

Figure 4. (**a–f**) Representative autoradiographs of some EMSAs that have been used for the determination of the apparent K_D's of RutR binding to wild type (WT) and mutant RutR binding sites present on 46-bp long DNA duplexes. All the variant binding sites shown here are symmetrically substituted at position +4 and −4. The molecular structure of the base pair is also shown, with indication of the hydrophobic methyl group of thymine (triangle) in the major groove, and of the groups that may act as potential donors or acceptors in hydrogen bond formation. RutR concentrations used are indicated in nM. The positions of free DNA (F) and of RutR-bound duplexes (B) are indicated. With the double T·A/A·T mutant, DNA binding was only observed at the highest protein concentrations used and did not produce a specific complex, but aggregates that remained in the well. (**g**) Binding profiles of the EMSAs shown in (a–f).

The apparent bending angle of free DNA molecules (intrinsic bending) and of RutR·DNA complexes was calculated from the relative mobilities on 8% acrylamide gels as described (34,35). The results indicate a slight intrinsic bending of ~24°, that may be explained by the in phase stretches of A·T bps in the cloned 36-bp fragment comprising the RutR binding site and flanking sequences, and an apparent bending angle of ~37° for the RutR·DNA complexes (Figure 5d).

Table 1. K_D and K_{Drel} values for double substitution mutants of the RUT box

Position	Wild-type bp	Double substitution	K_D (nM)	K_{Drel} [a]
−1/+1	T·A/A·T	G·C/C·G	42	1.2
		I·C/C·I	19	0.5
−3/+3	C·G/G·C	G·C/C·G	447	12.7
		T·A/A·T	20	0.6
		A·T/T·A	989	28.3
−4/+4	C·G/G·C	G·C/C·G	130	3.7
		T·A/A·T	102	2.9
		A·T/T·A	ND[b]	–
		U·A/A·U	202	5.8
		A·U/U·A	114	3.2
−5/+5	A·T/T·A	T·A/A·T	101	2.9
		G·C/C·G	422	12.1
		C·G/G·C	554	15.8

[a]K_{Drel} is the relative K_D value compared with the K_D of binding to the WT oligonucleotide duplex.
[b]No specific complex formation detectable.

Uracil but not thymine abolishes RutR binding at physiologically relevant concentrations

Shimada *et al.* (2) reported previously that both uracil and thymine abolish the binding of RutR to its target sites. However, these experiments were performed with a single concentration of the various potential effector molecules tested and, furthermore, a careful inspection of the published data reveals that thymine at 100 μM has at most a small effect only.

To better evaluate the effect of uracil and thymine as potential physiologically relevant effector molecules of RutR binding, we performed EMSAs with RutR binding to DNA fragments bearing the *car*P1, *rutA–rutR* and *ygiF* control regions in the presence of increasing concentrations of either uracil or thymine (Figure 6). The results clearly indicate that only uracil inhibits complex formation with the *car*P1 operator (Figure 6a). An inhibition of 50% ($I_{0.5}$) was observed at ~100 nM uracil, and complex formation was completely abolished at about 130 nM. In contrast, thymine had nearly no effect, even at 1.25 mM. Similarly, binding of RutR to

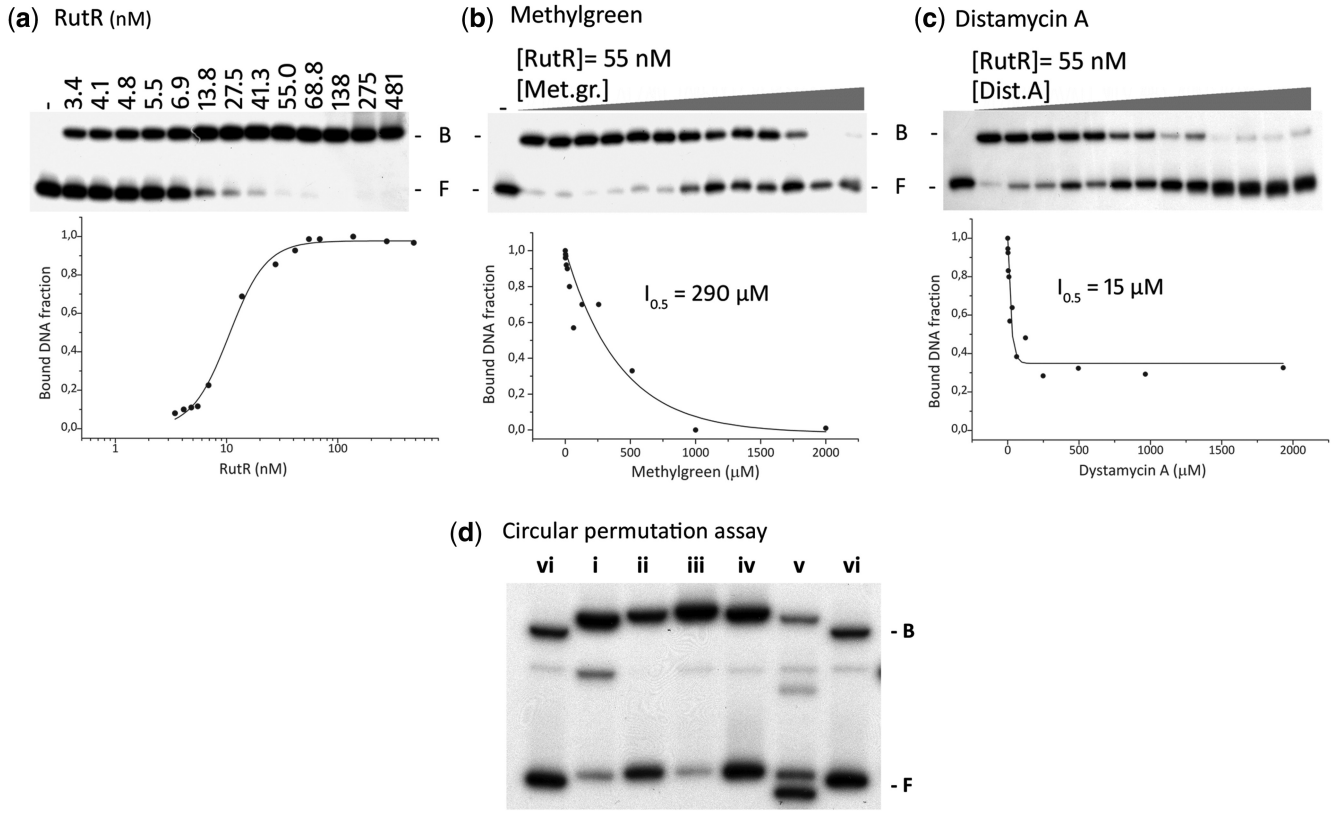

Figure 5. (**a**) Representative autoradiograph of an EMSA with RutR binding to the 162 bp *car*P1 operator fragment and corresponding binding profile. RutR concentrations are indicated in nM. The position of free DNA (F) and of RutR-bound DNA (B) is indicated. (**b** and **c**) Interference effect on RutR binding to the 162-bp *car*P1 operator fragment by increasing concentrations of the major and minor groove specific ligands methylgreen and distamycin A, respectively. The first lane of each panel is without RutR; all the other lanes contain RutR at 55 nM. (**d**) EMSA on 8% acrylamide of RutR binding to a set of permuted fragments bearing the RutR binding site of the *car*P1 control region generated from pBendRUT.

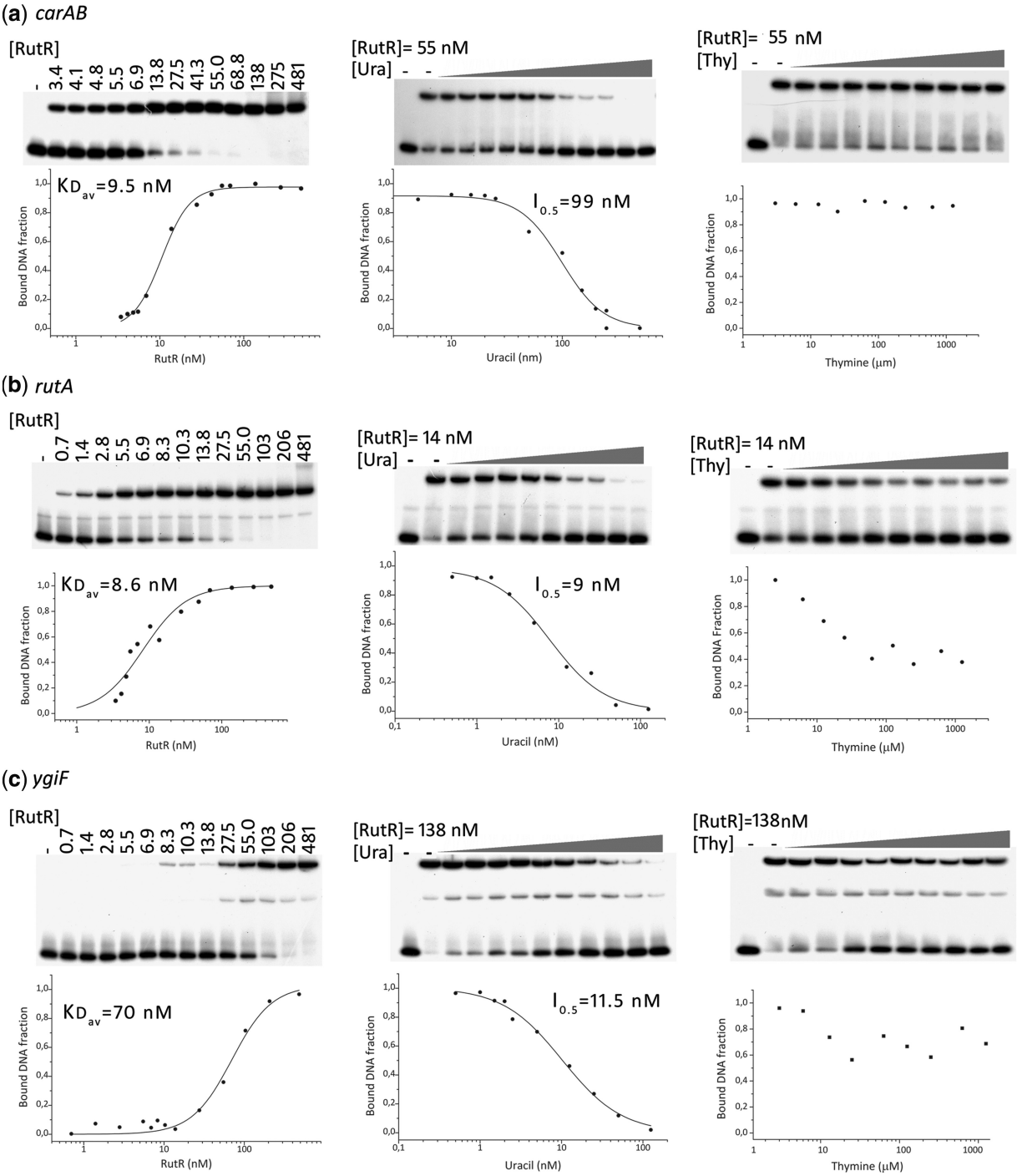

Figure 6. Representative EMSAs and the corresponding binding profiles of RutR binding to (**a**) the *carAB*, (**b**) the *rutA–rutR* and (**c**) the *ygiF* control region in the absence of potential ligands, and in the presence of increasing concentrations of uracil (Ura, in nM) or thymine (Thy, in μM). The first lane of each panel is without RutR. The position of free DNA (F) and of RutR-bound DNA (B) is indicated.

the *rutA–rutR* and *ygiF* fragments resulted in the formation of a single complex and occurred with a comparable affinity for the *rutA–rutR* and *carAB* fragments (average K_D of 8.6 and 9.5 nM, respectively), but was significantly weaker for the *ygiF* operator (average K_D of 70 nM; Figure 6b and c). Uracil inhibited complex formation with the *rutA–rutR* and *ygiF* operators at a comparable concentration of the ligand with an $I_{0.5}$ of ~9.0 and 11.5 nM, respectively, which is significantly lower than for the *car*P1 fragment. Again, thymine had a much smaller effect, culminating in about 50% inhibition at 100 μM. Therefore, we may conclude that uracil but not thymine is the physiologically relevant effector molecule of RutR.

A model of the RutR·*car*P1 complex

A comparison of the sequence conservation of RutR at the positions known to contact the DNA in the TetR and QacR co-crystal structures (6,36) indicates a higher similarity with the latter (Figure 7c). This is corroborated at the structural level by a better superimposition of the Cα atoms of the HTH motif of RutR and QacR, which superimpose nearly perfectly (r.m.s.d. = 0.84Å; Figure 8) and, furthermore, the DNA binding site of RutR is also more similar to the QacR than to the TetR target sequence. Therefore, we used the RutR protein structure and the QacR·IR1 co-crystal structure to build a model of the RutR·*car*P1 operator complex (Figure 7a and b).

Two QacR dimers bind cooperatively to the 28-bp *qacA* operator, whereas our results indicate that RutR likely binds as a single dimer to a palindromic binding site. When the HTH motif of one monomer of RutR is superimposed with the A-distal monomer of QacR in the co-crystal structure, similar contacts are made with the DNA (Figures 7 and 8). There are only two striking differences: (i) glycine 37 of QacR is a threonine (Thr52) in RutR and makes a steric clash in the model (Figure 8; see 'Discussion' section) and (ii) the second pair of monomers is not at all aligned in this overlay and does not make contact with DNA in the RutR·*car*P1 operator model (Figure 8). This underscores major differences in the way RutR and QacR dimers contact the DNA. QacR binding results in global undertwisting and major groove widening, but the operator DNA is bent by 3° only (6). The untwisting and major groove widening are the structural basis for the cooperative binding of two QacR dimers. In contrast, the model indicates that the *car*P1 target will have to be bent by about 50° to allow the simultaneous interaction of both subunits of the RutR dimer with the two half-sites of the *car*P1 operator. This observation is in agreement with the experimental results of the DNA bending analysis that indicates a bending

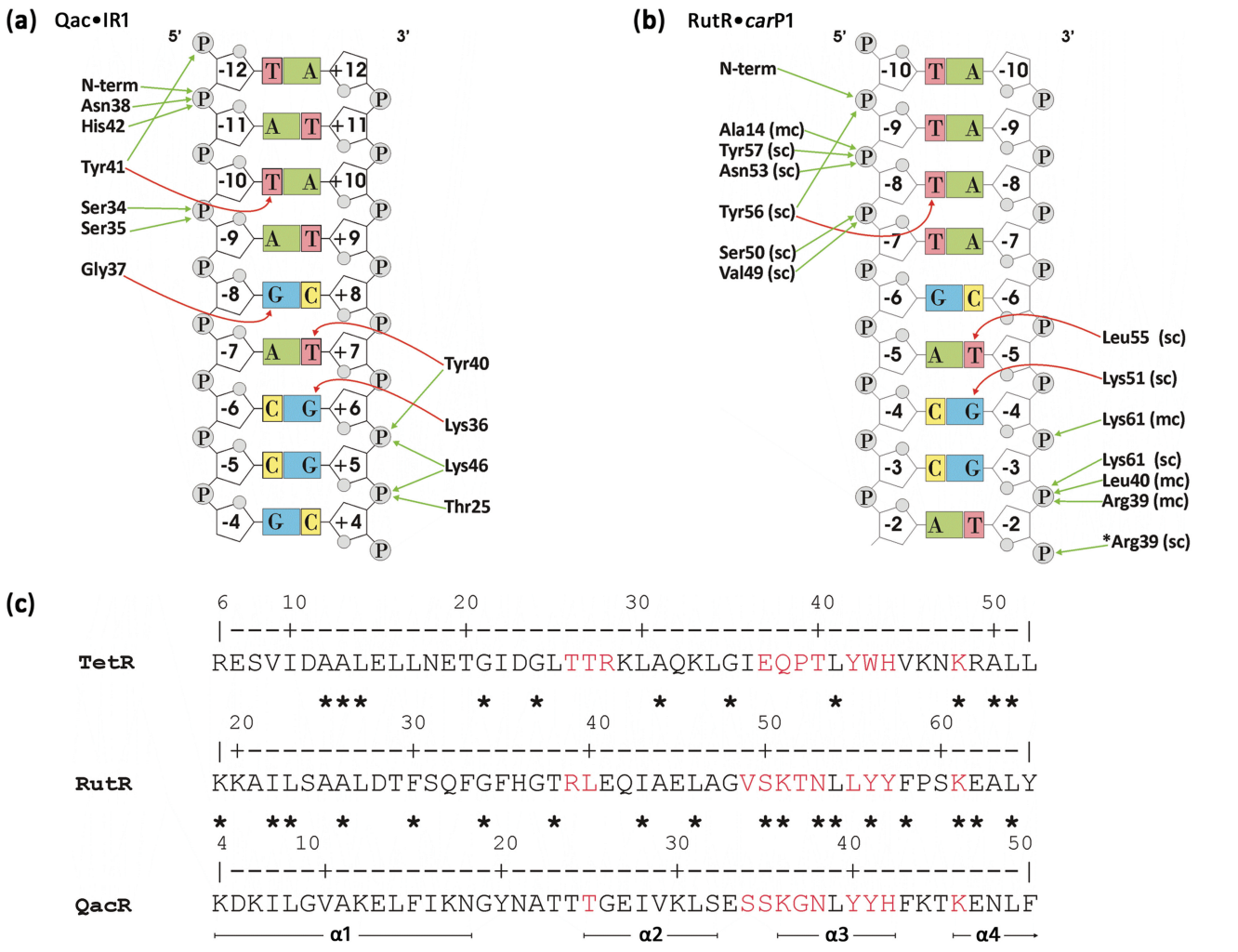

Figure 7. QacR and RutR–DNA contacts. (**a**) Protein–DNA contacts of the promoter distal subunit A of QacR with the IR1 operator deduced from the co-crystal structure (6). Arrows indicate contacts with phosphates (green) or bases (red). (**b**) Model of the RutR–*car*P1 operator DNA contacts built on basis of the overlay of the DNA binding HTH motif of RutR with QacR in the co-crystal structure. (**c**) Amino acid sequence alignment of the DNA-binding motif of TetR, RutR and QacR. Residues of TetR and QacR that are known to contact the DNA are indicated in red. Asterisks in between two lines indicate sequence identity.

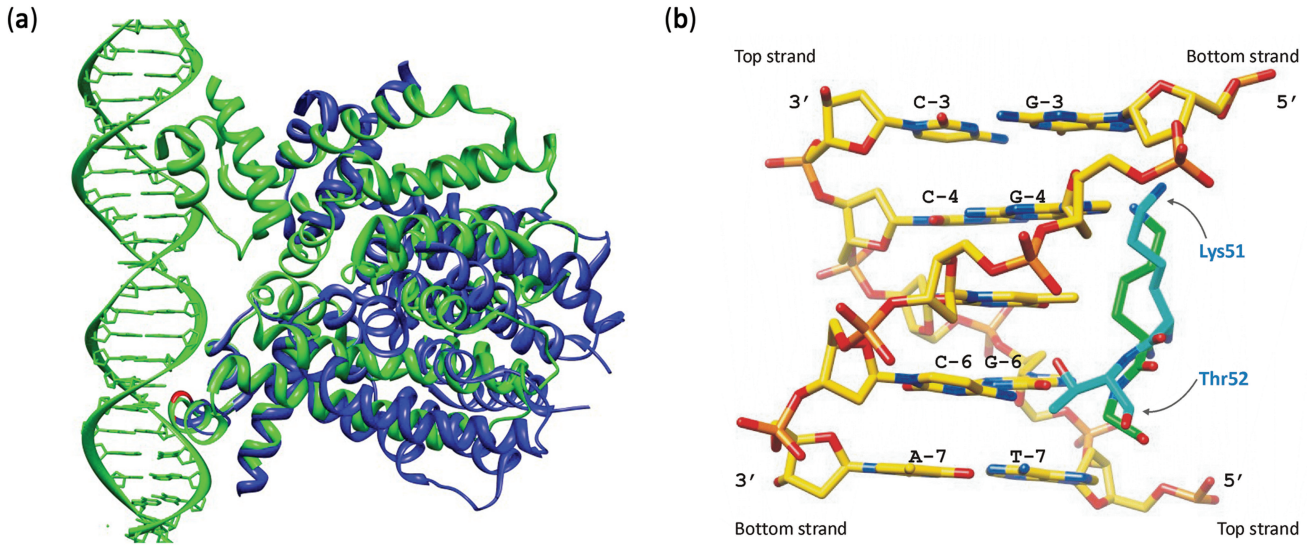

Figure 8. (**a**) Ribbon representation of the binding of a QacR dimer to two successive major groove segments of the IR1 operator (in green), with the superimposed structure of RutR (in blue). The main chain around Thr 52 (residue 51–53) in RutR is colored in red. (**b**) Detailed picture of the RutR-QacR overlay in the region surrounding Thr52 of RutR. The residues Lys51 and Thr52 are shown in cyan; their homologues Lys36 and Gly37 in QacR are shown in green and the DNA (from −7 to −3) is shown in gold.

angle of ~37° for the RutR·*car*P1 operator complex. It is also reminiscent of the TetR·DNA complex, where a 17° bend towards the protein is used to optimize the positioning of the HTH motifs for interactions with the two half-sites of the operator (4,36).

Figure 8 shows a comparison of the contacts deduced from the QacR·IR1 co-crystal structure and the contacts proposed for the RutR·*car*P1 operator complex. From the model it appears that six phosphates and three bases in one half-site of the *car*P1 operator may be directly contacted by RutR. Similar contacts may be expected in the symmetrical half-site. Thus, on the top strand the phosphate 5′ to T-9 may be contacted by the side chain of Tyr56 and possibly by the N-terminus of RutR. This N-terminus is oriented differently in the RutR structure as compared to the N-terminus of QacR in the co-crystal, but the region shows high B-factors and may be reoriented differently in the co-crystal. The phosphate 5′ to T-8 appears to be contacted by the side chains of Asn53 and Tyr57 and the main chain of Ala14, and the phosphate 5′ to T-7 by the side chains of Val49 and Ser50. On the bottom strand the phosphate 5′ to G-4 may be contacted by the main chain amide nitrogen of Lys61 and the phosphate 5′ to G-3 by the main chain of Arg39 (Cα) and Leu40 (amide nitrogen), and the side chain of Lys61. Finally, it is possible that the side chain of Arg39 interacts with the phosphate 5′ to T-5 of the bottom strand. It is worth noticing that this pattern is in full agreement with the results of the phosphate ethylation premodification interference experiments. All phosphates that appear to be contacted in the model (Figure 7b) negatively interfered with RutR binding upon ethylation (Figure 3) and the strongest effects were observed for the phosphates that are contacted by more than one amino acid residue in the model.

Base-specific contacts may be established between the residue T-8 of the top strand and the side chain of Tyr56, residue T-5 of the bottom strand and the side chain of Leu55 and between residue G-4 of the bottom strand and the side chain of Lys51. Notice that the removal of these residues in the missing contact probing assays resulted in a pronounced drop in the binding affinity (Figure 3).

Effects of single amino acid substitutions in the DNA-binding domain of RutR on DNA binding affinity and sequence specificity

To test the validity of the model presented above for the RutR·*car*P1 complex, we constructed several single amino acid substitution mutants of RutR and analyzed the binding of the cognate purified His-tagged proteins to the 46 bp consensus duplex and derivatives thereof (saturation mutagenesis) bearing a symmetrical substitution in both half-sites at the position of the presumed contacts. If the side chain of a particular amino acid of RutR interacts with the DNA, substituting alanine for that residue is expected to cause a decrease in binding affinity, and furthermore, if the contact is established with a base-specific group, the preference for that base pair is expected to be altered as well. Four residues of the DNA-binding domain that contact base-specific groups or phosphate residues according to the model were substituted with alanine: Lys51 (K51A), Leu55 (L55A), Tyr56 (Y56A) and Lys61 (K61A). All four mutants showed a significantly reduced affinity for the 46 bp consensus duplex (Table 2). The drop was most pronounced for the L55A (70-fold) and K61A (43-fold) mutants. According to the model, these residues make base-specific (T-5/+5) and backbone (two consecutive phosphates 5′ to positions 3 and 4) contacts, respectively.

Table 2. K_{Drel} values of RutR mutant proteins to the consensus duplex and to symmetrical mutant derivatives thereof

RutR	K_{Drel}	
Consensus duplex		
WT	1.0	
K51A	14.3	
L55A	70.2	
Y56A	17.2	
K61A	43.0	
T52A	1.2	
T52G	1.4	
RutR	Duplex	K_{Drel}
Symmetrical mutant derivatives		
L55A	−5/+5	
	A·T/T·A	1.0
	T·A/A·T	1.0
	G·C/C·G	1.4
	C·G/G·C	4.3
K51A	−4/+4	
	C·G/G·C	1.0
	G·C/C·G	1.3
	T·A/A·T	2.8
	A·T/T·A	ND[a]
K61A	−4/+4	
	C·G/G·C	1.0
	G·C/C·G	10.4
	T·A/A·T	5.5
	A·T/T·A	ND[a]

[a]No specific complex formation detectable.

Lys61 is not part of the HTH motif but the residue is highly conserved among TetR family members and supposedly involved in correctly orienting the HTH motifs with respect to the major groove segments of the target site (see 'Discussion' section). The substitution of Lys51 and Tyr56, contacting a G (position 4) and a T (position 8) residue, respectively, resulted in a 14- and 17-fold drop in the affinity for the consensus duplex. In contrast, the substitution of either alanine or glycine for Thr52 had little effect on the binding to the consensus duplex (Table 2, see 'Discussion' section).

The K51A and L55A mutant RutR proteins were further tested for the binding specificity. EMSAs with these mutant RutR proteins binding to the cognate DNA duplexes representing a saturation mutagenesis of positions 4 and 5, respetively, indicated a remarkable decrease in the binding specificity (Table 2). For RutR-L55A the largest difference in the relative K_D was 4.3 (instead of 15.8 for wild type RutR). Similarly, the binding of the K51A mutant protein occurred with a similar affinity to three out of the four duplexes. As also observed with wild-type RutR, no specific complex formation was detected with the substitution of A·T for C·G. This observation futher corroborates the hypothesis that the methyl group of a T residue at this particular position exerts an additional negative effect on nearby contacts (see above; Figure 4 and Table 1). In contrast, binding of RutR-K61A still showed a strong preference for the C·G/G·C pairs at position −4/+4, as expected if K61 exclusively contacts phosphate groups, as proposed in the model.

DISCUSSION

The RutR·*car*P1 complex

Members of the large TetR family of transcriptional regulators show little overall sequence homology and bind a wide variety of ligands as allosteric co-factors (4). However, they all exhibit structural similarities and share a highly homologous N-terminal DNA-binding domain of about 45 residues. Structures of TetR (pdb 1QPI), QacR (pdb 1JT0), IcaR (pdb2ZCM), RutR (YcdC; pdb 1PB6) and some other family members indicate that in the monomer architecture this region adopts a common 3D structure consisting of a three helix bundle that contains a HTH DNA-binding motif composed of helices α2 and α3 (for a review see (4; Figure 7c). A common feature of TetR-family members is the unusually short recognition helix α3 of seven residues that are fully engaged in DNA binding (Figure 7). Phosphates and base-specific groups that play an importants role in the formation of RutR·DNA complexes were identified with various premodification binding interference techniques and saturation mutagenesis of particular positions of the target site (Figures 3 and 4, Table 1). This information, combined with the high degree of sequence conservation in the HTH motif of the RutR and QacR proteins and in their DNA targets allowed us to build a model of the RutR·DNA complex based on the co-crystal structure of the QacR·DNA complex (Figure 7). This model reflects the similarities of the contacts made by these two proteins; it was further tested with binding studies of alanine substitution mutants of residues that are expected to contact either phosphate or base-specific groups with their side-chain. The side chains of Val49 and Ser50 likely contact the phosphate of T-7 of the *car*P1 operator, similar to the contacts made by Ser34 and Ser35 of QacR. The side chain of Lys51 contacts the G-4 base, as does the conserved Lys36 of QacR. Both the observed drop in binding affinity and the loss of sequence specificity at position 4 of the target site in the binding of the RutR-K51A mutant protein corroborate the contact between the side-chain of Lys51 and the G residue in position −4/+4 (Table 2). The side chain of Asn53 contacts the phosphate of T-8, similar to the conserved Asn38 of QacR. The side chain of Leu55 appears to be well positioned to contact the T-5 base, similar to the T residue contacted by the side chain of Tyr40 of QacR. Again, analyses of the binding properties of the RutR-L55A mutant protein corroborate this view. The side chain of Tyr56 can be positioned in such a way (same rotamer as Tyr41 in QacR) that it may contact the phosphate 5′ of T-9 and the base T-8 of the top strand, identical to the two contacts established by the conserved Tyr41 of QacR. The significantly reduced binding affinity measured fot the RutR-Y56A mutant protein highlights the energetic contribution of Tyr56 to complex formation. Tyr57 contacts the phosphate 5′ of T-8, similarly to His42 of QacR. Finally, the main chain amide nitrogen of Lys61 appears to be well positioned to contact the phosphate 5′ of G-4, whereas its side chain might contact the phosphate 5′ of G-3. Both contacts

are similar to the phosphate contacts of the conserved Lys46 of QacR. Again, the strong reduction in binding affinity of the K61A mutant protein indicates an important energetic contribution of the residue in complex formation, as may be expected for interactions with negatively charged phosphates. The residues equivalent to position Leu55 of RutR (Tyr in 74% of all TetR-family members) and Tyr57 (His or Tyr in 98% of all TetR-family members), both located in the recognition helix α3, and Lys61 (Lys in 77% of all TetR-family members), located in α4 outside the HTH motif, are all well conserved and probably serve to orient the HTH motif to interact with the DNA major groove and anchor the protein to the operator (4). The strong negative effect of the RutR-K61A substitution on DNA binding corroborates the involvement of Lys61 in complex formation. Interestingly, the residue at position 55 (RutR numbering) is generally a Tyr that makes contacts with both a phosphate residue and a T base in the QacR and TetR structures. The side chain of Leu55 at this position of RutR is quite different and may contact the T-5 base of the bottom strand, but does not appear to interact with the backbone. The strongly reduced sequence specificity in the binding of RutR-L55A to a set of RutR binding sites mutated at position 5 is fully compatible with this proposal.

The nature of the amino acid residue in positions equivalent to 51, 52, 53 and 56 of RutR is quite variable among the TetR family-members. In the QacR and TetR structure, these residues make contact with bases, except for Asn38 of QacR that contacts a phosphate only. Therefore, the nature of the residues present at these positions likely endows DNA binding sequence-specificity to each regulator. QacR and RutR show remarkable sequence conservation at these positions and their DNA target sequences show a high degree of sequence identity (Figure 7). Thus Lys51, Asn53 and Tyr56 are conserved and in the model, Asn53 of RutR also appears to interact with a phosphate only, as does Asn38 of QacR. Most interestingly, position 52 of RutR is a Thr that aligns with Gly37 of QacR. From the Qac·IR1 co-crystal structure it was deduced that any side chain at this position would clash with any base of the operator at the position of the G residue contacted by the amide nitrogen of Gly37 and its Cα that are both close to the O^6 of the base, thereby explaining a preference for G over A at this position of the IR1 operator (6). Gly37 of QacR is important for repression since it contacts the G residue right at the start of *qacA* transcription initiation. In the RutR·*car*P1 operator DNA model, Thr52 would clash with the base G-6 of the top strand, but the residue could also be squeezed between the stacked base pairs at −6 and −7 and interact with T-7 of the top strand, for which we observed a strong negative effect on RutR binding in the missing contact probing. However, substituting either alanine or glycine for Thr52 had hardly any effect on the binding affinity (Table 2). This is an early indication that the real structure of the complex must locally deviate from the model, likely due to an induced fit of RutR and its operator upon binding. Evidently, it will be necessary to solve the structure of a RutR-operator co-crystal to obtain a more detailed and accurate picture of all the interactions. Finally, it is a striking observation that in contrast to many other transcriptional DNA-binding regulators, no water molecules are incorporated into the protein–DNA interface of TetR and QacR-operator complexes. It will be interesting to determine whether this is also the case for RutR.

Co-factor specificity and mode of action of RutR

In vitro the binding of RutR to various targets is strongly inhibited in the presence of sub micromolar concentrations of uracil (Figure 6). In contrast, thymine had only a small effect, even at much higher concentrations. Therefore, it appears that uracil is the real physiologically important effector molecule for RutR. This difference in the effector potential of uracil and thymine, which differ by the C^5 methyl group only, must reflect either a reduced binding affinity of thymine or a deficiency in the signal transduction from the C-terminal effector-binding site to the N-terminal HTH motif. This striking difference in the effect of two rather similar and small effector molecules is in striking contrast with the multidrug binding capacity of various TetR-family members (4,37).

All TetR-family members of which the function is known are repressors and effector binding results in their dissociation from the DNA (4,6,37). They bind either in overlap with the conserved core promoter elements or in overlap with the startpoint of transcription and inhibit the initial binding of RNA polymerase or the transition of the closed complex to a transcriptionally productive state, as does QacR. This is different for RutR in the control of *car*P1 activity, where RutR is clearly required for full derepression of *car*P1 activity in the absence of extra uracil in the medium (2) and, furthermore, the RutR binding site is located rather far upstream of the *car*P1 promoter and comprised within the region that gets wrapped around hexameric PepA (Figure 1). Therefore, RutR most likely acts as an anti-repressor rather than as a repressor or activator, though this remains to be demonstatated. The mode of action of RutR in the control of *car*P1 activity is also very different from its role in autoregulation and in negative control of the σ^s-dependent *gadAXW* and *gadBC* operons involved in glutamate transport and glutamate-dependent acid resistance, where RutR binds downstream of the transcription start and possibly acts as a roadblock, and in the activation of the catabolic *rutABCDEFG* operon from a σ^{54}-dependent promoter (2). How RutR fits precisely into the intricate regulatory pattern of *car*P1 control and how it may interact/interfere with the other regulatory proteins binding to the *carAB* control region is not yet fully elucidated. These issues are presently addressed with *in vivo* and *in vitro* approaches, but are beyond the scope of this article.

SUPPLEMENTARY DATA

Supplementary Data are available at NAR Online.

ACKNOWLEDGEMENTS

We acknowledge the excellent technical assistance of Nadine Huysveld and thank Dr ir. Eveline Peeters for the help with the protein purifications and for critical reading of the article.

FUNDING

Research-Foundation-Flanders (FWO-Vlaanderen G.0429.06); Research Council of the Brussels University (OZR1624, OZR1818); Flanders Interuniversity Institute for Biotechnology (VIB); Belgian Federal Science Policy Office (DWTC: Prodex project ESA-AO-2004-070); Vlaamse Gemeenschapscommissie. Funding for open access charge: Research-Foundation-Flanders (FWO-Vlaanderen G.0429.06).

Conflict of interest statement. None declared.

REFERENCES

1. Loh,K.D., Gyaneshwar,P., Papadimitriou,M.E., Fong,R., Kim,K.-S., Parales,R., Zhou,Z., Inwood,W. and Kustu,S. (2006) A previously undescribed pathway for pyrimidine catabolism. *Proc. Natl Acad. Sci. USA*, **103**, 5114–5119.
2. Shimada,T., Hirao,K., Kori,A., Yamamoto,K. and Ishihama,A. (2007) RutR is the uracil/thymine-sensing master regulator of a set of genes for synthesis and degradation of pyrimidines. *Mol. Mocrobiol.*, **66**, 744–757.
3. Shimada,T., Ishihama,A., Busby,S.J.W. and Grainger,D.C. (2008) The *Escherichia coli* RutR transcription factor binds at targets within genes as well as intergenic regions. *Nucleic Acids Res.*, **36**, 3950–3955.
4. Ramos,J.L., Martínez-Bueno,M., Molina-Henares,A.J., Terán,W., Watanabe,K., Zhang,X., Gallegos,M.T., Brennan,R. and Tobes,R. (2005) The TetR family of transcriptional repressors. *Microbiol. Molec. Biol. Rev.*, **69**, 326–356.
5. Quiñones,B., Pujol,C.J. and Lindow,S.E. (2004) Regulation of AHL production and its contribution to epiphytic fitness in *Pseudomonas syringae*. *Mol. Plant-Microbe Interact.*, **17**, 521–531.
6. Schumacher,M.A., Miller,M.C., Grkovic,S., Brown,M.H., Skurray,R.A. and Brennan,R.G. (2002) Structural basis for cooperative DNA binding by two dimers of the multidrug-binding protein QacR. *EMBO J.*, **21**, 1210–1218.
7. Charlier,D. and Glansdorff,N. (2004) Biosynthesis of arginine and polyamines. In Curtiss,R. III (ed.), *Eco-Sal – Escherichia coli and Salmonella: Cellular and Molecular Biology*, Chapter 3.6.1.10, ASM Press, Wahington, DC.
8. Bouvier,J., Patte,J. and Stragier,C.P. (1984) Multiple regulatory signals in the control region of the *Escherichia coli carAB* operon. *Proc. Natl Acad. Sci. USA*, **81**, 4139–4143.
9. Piette,J., Nyunoya,H., Lusty,C.J., Cunin,R., Weyens,G., Crabeel,M., Charlier,D., Glansdorff,N. and Piérard,A. (1984) DNA sequence of the *carA* gene and of the control region of *carAB*: tandem promoters, respectively controlled by arginine and the pyrimidines, regulate the synthesis of carbamoylphosphate synthetase in *Escherichia coli* K-12. *Proc. Natl Acad. Sci. USA*, **81**, 4134–4138.
10. Charlier,D., Weyens,G., Roovers,M., Piette,J., Bocquet,C., Piérard,A. and Glansdorff,N. (1988) Molecular interactions in the control region of the *carAB* operon encoding *Escherichia coli* carbamoylphosphate synthetase. *J. Mol. Biol.*, **204**, 867–877.
11. Charlier,D., Roovers,M., Van Vliet,F., Boyen,A., Cunin,R., Nakamura,Y., Glansdorff,N. and Piérard,A. (1992) Arginine regulon of *Escherichia coli* K-12. A study of repressor-operator interactions and of *in vitro* binding affinities versus *in vivo* repression. *J. Mol. Biol.*, **226**, 367–386.
12. Wang,H., Glansdorff,N. and Charlier,D. (1998) The arginine repressor of *Escherichia coli* K-12 makes direct contacts to minor and major groove determinants of the operators. *J. Mol. Biol.*, **277**, 805–824.
13. Han,X. and Turnbough,C.L. Jr. (1998) Regulation of *carAB* expression in *Escherichia coli* occurs in part through UTP-sensitive reiterative transcription. *J. Bacteriol.*, **180**, 705–713.
14. Charlier,D., Roovers,M., Gigot,D., Huysveld,N., Piérard,A. and Glansdorff,N. (1993) Integration host factor (IHF) modulates the expression of the pyrimidine-specific promoter of the *carAB* operons of *Escherichia coli* K12 and *Salmonella typhimurium* LT2. *Mol. Gen. Genet.*, **237**, 273–286.
15. Charlier,D., Hassanzadeh,G., Kholti,A., Gigot,D., Piérard,A. and Glansdorff,N. (1995) *carP*, involved in pyrimidine regulation of the *Escherichia coli* carbamoylphosphate synthetase operon encodes a sequence-specific DNA-binding protein identical to XerB and PepA, also required for resolution of ColE1 multimers. *J. Mol. Biol.*, **250**, 392–406.
16. Devroede,N., Thia-Toong,T.-L., Gigot,D., Maes,D. and Charlier,D. (2004) Purine and pyrimidine-specific repression of the *Escherichia coli carAB* operon are functionally and structurally coupled. *J. Mol. Biol.*, **336**, 25–42.
17. Devroede,N., Huysveld,N. and Charlier,D. (2006) Mutational analysis of intervening sequences connecting the binding sites for integration host factor, PepA, PurR, and RNA polymerase in the control region of the *Escherichia coli carAB* operon, encoding carbamoylphosphate synthase. *J. Bacteriol.*, **188**, 3236–3245.
18. Nguyen Le Minh,P., Devroede,N., Massant,J., Maes,D. and Charlier,D. (2009) Insights into the architecture and stoichiometry of *Escherichia coli* PepA•DNA complexes involved in transcriptional control and site-specific DNA recombination by atomic force microscopy. *Nucleic Acids Res.*, **37**, 1463–1476.
19. Kholti,A., Charlier,D., Gigot,D., Huysveld,N. and Glansdorff,N. (1998) *pyrH*-encoded UMP-kinase directly participates in pyrimidine-specific modulation of promoter activity in *Escherichia coli*. *J. Mol. Biol.*, **280**, 571–582.
20. Charlier,D., Kholti,A., Huysveld,N., Gigot,D., Maes,D., Thia-Toong,T.-L. and Glansdorff,N. (2000) Mutational analysis of *Escherichia coli* PepA, a multifunctional DNA-binding aminopeptidase. *J. Mol. Biol.*, **302**, 411–426.
21. Marco-Marín,C., Gil-Otiz,F. and Rubio,V. (2005) The crystal structure of *Pyrococcus furiosus* UMP kinase provides insights into catalysis and regulation in microbial nucleotide biosynthesis. *J. Mol. Biol.*, **352**, 438–454.
22. Kim,J., Zwieb,C., Wu,C. and Adhya,S. (1989) Bending of DNA by gene-regulatory proteins: construction and use of a DNA bending vector. *Gene*, **85**, 15–23.
23. Higuchi,R., Krummel,B. and Saiki,R.K. (1988) A general method for *in vitro* preparation and specific mutagenesis of DNA fragments: study of protein and DNA interactions. *Nucleic Acids Res.*, **16**, 7351–7367.
24. Peeters,E., Wartel,C., Maes,D. and Charlier,D. (2007) Analysis of the DNA-binding sequence specificity of the archaeal transcriptional regulator Ss-LrpB from *Sulfolobus solfataricus* by systematic mutagenesis and high resolution contact probing. *Nucleic Acids Res.*, **35**, 623–633.
25. Peeters,E., Thia-Toong,T.-L., Gigot,D., Maes,D. and Charlier,D. (2004) Ss-LrpB, a novel Lrp-like regulator of *Sulfolobus solfataricus* P2, binds cooperatively to three conserved targets in its own control region. *Mol. Microbiol.*, **54**, 321–336.
26. Maxam,A.M. and Gilbert,W. (1980) Sequencing end-labeled DNA with base-specific chemical cleavages. *Methods Enzymol.*, **65**, 499–560.
27. Emsley,P. and Cowtan,K. (2004) Coot: model-building tools for molecular graphics. *Acta Crystallogr. D Biol. Crystallogr.*, **60**, 2126–2132.
28. Pettersen,E.F., Goddard,T.D., Huang,C.C., Couch,G.S., Greenblatt,D.M., Meng,E.C. and Ferrin,T.E. (2004) UCSF Chimera: a visualization system for exploratory research and analysis. *J. Comput. Chem.*, **25**, 1605–1612.
29. Kuwabara,M.D. and Sigman,D.S. (1987) Footprinting DNA-protein complexes *in situ* following gel retardation assays using 1, 10-phenathroline-copper ion: *Escherichia coli* RNA-polymerase-*lac* promoter complexes. *Biochemistry*, **26**, 7234–7238.

30. Tullius,T.D. and Dombroski,B.A. (1986) Hydroxyl radical 'footprinting': high-resolution information about DNA-protein contacts and application to λ repressor and Cro protein. *Proc. Natl Acad. Sci. USA*, **83**, 5469–5473.
31. Siebenlist,U. and Gilbert,W. (1980) Contacts between *Escherichia coli* RNA polymerase and an early promoter of phage T7. *Proc. Natl Acad. Sci. USA*, **77**, 122–126.
32. Brunelle,A. and Schleif,R.F. (1987) Missing contact probing of DNA-protein interactions. *Proc. Natl Acad. Sci. USA*, **84**, 6673–6676.
33. Kopka,M.L., Yoon,C., Goodsell,D., Pjura,P. and Dickerson,R.E. (1985) The molecular origin of DNA-drug specificity in netropsin and distamycin. *Proc. Natl Acad. Sci. USA*, **82**, 1276–1380.
34. Wu,H.-M. and Crothers,D.M. (1984) The locus of a sequence-directed and protein-induced DNA bending. *Nature*, **308**, 509–513.
35. Thompson,J.F. and Landy,A. (1988) Empirical estimation of protein-induced DNA-bending angles: applications to lambda site-specific recombination complexes. *Nucleic Acids Res.*, **20**, 9678–9705.
36. Orth,P., Schnappinger,D., Hillen,W., Saenger,W. and Hinrichs,W. (2000) Structural basis of gene regulation by the tetracycline inducible Tet repressor-operator system. *Nature Struct. Biol.*, **7**, 215–219.
37. Jeng,W.-Y., Ko,T.-P., Liu,C.-I., Guo,R.-T., Liu,C.-L., Shr,H.-L. and Wang,A.H.-J. (2008) Crystal structure of IcaR, a repressor of the TetR family implicated in biofilm formation in *Staphylococcus epidermis*. *Nucleic Acids Res.*, **35**, 1567–1577.